

Two-phase forest inventory using very-high-resolution laser scanning



Henrik J. Persson ^{*}, Kenneth Olofsson, Johan Holmgren

Department of Forest Resource Management, Swedish University of Agricultural Sciences (SLU), 901 83 Umeå, Sweden

ARTICLE INFO

Editor: Marie Weiss

Keywords:

Forestry
Laser scanning
Hybrid inference
Forest inventory
Sampling

ABSTRACT

In this study, we compared a two-phase laser-scanning-based forest inventory of stands versus a traditional field inventory using sample plots. The two approaches were used to estimate stem volume (VOL), Lorey's mean height (H_L), Lorey's stem diameter (D_L), and VOL per tree species in a study area in Sweden. The estimates were compared at the stand level with the harvested reference values obtained using a forest harvester. In the first phase, a helicopter acquired airborne laser scanning (ALS) data with >500 points/m² along 50-m wide strips across the stands. These strips intersected systematic plots in phase two, where terrestrial laser scanning (TLS) was used to model D_L for individual trees. In total, phase two included 99 plots across 10 boreal forest stands in Sweden (lat 62.9° N, long 16.9° E). The single trees were segmented in both the ALS and TLS data and linked to each other. The very-high-resolution ALS data enabled us to directly measure tree heights and also classify tree species using a convolutional neural network. Stem volume was predicted from the predicted DBH and the estimated height, using national models, and aggregated at the stand level. The study demonstrates a workflow to derive forest variables and stand-level statistics that has potential to replace many manual field inventories thanks to its time efficiency and improved accuracy. To evaluate the inventories, we estimated bias, RMSE, and precision, expressed as standard error. The laser-scanning-based inventory provided estimates with an accuracy considerably higher than the field inventory. The RMSE was 17 m³/ha (7.24%), 0.9 m (5.63%), and 16 mm (5.99%) for VOL, H_L , and D_L respectively. The tree species classification was generally successful and improved the three species-specific VOL estimates by 9% to 74%, compared to field estimates. In conclusion, the demonstrated laser-scanning-based inventory shows potential to replace some future forest inventories, thanks to the increased accuracy demonstrated empirically in the Swedish forest study area.

1. Introduction

Remote sensing (RS) has become an invaluable resource for many forest-related applications. However, forestry companies in Sweden and practitioners worldwide rely widely on field sample plots as the main information source for design-based (DB) inventories used to generate descriptive statistics about forests. Field plots are manually inventoried, which is both costly and error-prone, since both subjective assessments and the use of generic models are required (the former, in particular, involve a dependence on personnel). The transition to a more-digital forestry includes frequent and objective monitoring, which to date only appears possible with the use of RS to acquire the necessary auxiliary data. To utilize the auxiliary data, a model-based (MB) or model-assisted (MA) framework is commonly used, where model parameters are estimated from a sample of field plots (Gregoire, 1998; McRoberts, 2006). The model is used to predict the target variable for all units in the auxiliary data (McRoberts et al., 2014). The accuracy, cost,

and possible frequency of acquiring RS data typically guide the user to select the most suitable sensor. This study focused on how a two-phase design with hybrid (HYB) inference, based on ALS and TLS, can be used for inventorying forests. This could both replace traditional DB inventories and provide a more accurate and precise estimate compared to current MB approaches, although it does not provide wall-to-wall data.

ALS has long been successfully used in forestry, and several countries have implemented operational, regular, national scanning programs (Kotivuori et al., 2016; Næsset et al., 2004; Nilsson et al., 2017; Persson et al., 2002; Waser et al., 2017). Historically, the sparse point densities made area-based approaches more feasible (Næsset, 1997a, 1997b), but current technical progress supports densities exceeding 10–100 points/m², which enable mapping of single-trees (Breidenbach et al., 2010; Lindberg and Holmgren, 2017; Olofsson and Holmgren, 2016; Sumnall et al., 2021; Yu et al., 2008). This has also improved the predictive accuracy and increased the challenges of evaluating the methods, due to the fact that both predictions and references may possess errors of

* Corresponding author.

E-mail address: Henrik.Persson@slu.se (H.J. Persson).

similar magnitudes (Persson and Ståhl, 2020). Field plots have historically been considered sufficiently accurate in the sense of providing reliable reference data for common forest variables, such as tree height, diameter, basal area, and stem volume (VOL). However, dense point clouds (sufficient to identify branches of single trees) from the latest laser scanners enable single-tree estimates that require even more accurate references than traditional field measurements can provide (Dalgente et al., 2011, 2014, 2019; Peuhkurinen et al., 2011). Modern harvesters appear feasible for this task, and they record measurements along the stem of single harvested trees, including diameter, length, and position, while tree species and damage are recorded based on the visual assessment of the harvester operator. Still, positional accuracy is limited (although current research may soon improve this). Both traditional field inventories and the modern harvesters use a global navigation satellite system (GNSS), which has a lower accuracy due to shadowing and interference when the antenna is located below a canopy (Frair et al., 2010; Valbuena et al., 2010). At the same time, the antenna is often located higher on a harvester compared to when using handheld receivers, which increases accuracy. Furthermore, the harvester removes the blocking trees, which improves the positioning accuracy of data from harvesters. These technical developments enable references that are more accurate when provided from a harvester.

The use of ALS is one alternative to meet the requirements of objective and frequent inventories. Yet despite its high accuracy, a number of challenges have hindered a complete transition to frequent, ALS-based inventories. Perhaps the most important reason may be that not all variables measured in the field have been possible to capture with ALS. Scanners with a single wavelength do not provide spectral information about tree species, and to gain cost efficiency and cover large areas, their point density is generally too low to extract geometric features for tree species classification. The accuracy of, e.g., VOL estimates from area-based ALS has, at best, been on a similar order as those obtained from field inventories (Breidenbach et al., 2010; Nilsson et al., 2017; Persson and Fransson, 2017; Tomppo et al., 2017; Yu et al., 2015). Furthermore, the prediction of tree stocking (stems per hectare) has often been limited due to the point density and airborne platform for ALS. The use of very-high-resolution (> 500 points/m²) ALS data provides more information about the shape of single trees (Burt et al., 2019; Holmgren et al., 2022; Lindberg and Holmgren, 2017), which may enable prediction of, e.g., tree species from a single-wavelength scanner (Hamraz et al., 2019; Marrs and Ni-Meister, 2019; Mizoguchi et al., 2019; Seidel et al., 2021; Terryn et al., 2020). Furthermore, the accuracy of detecting single trees and predicting forest attributes is expected to increase, and suppressed trees may be detectable. However, to obtain reference values about variables that cannot be directly measured from the air and hence must be estimated—e.g., diameter at breast height (DBH)—the use of ground references appears necessary. To improve the consistency, accuracy, and speed of such acquisitions, TLS is a suitable alternative to manual measurements. For practical use, single scans appear to be most feasible due to their speed (a few minutes) and simplicity (no merging of data required), which, however, may provide incomplete data from sample plots due to shadowed trees and hidden sectors. Nevertheless, the scanned trees are reconstructed at very high detail and constitute excellent references for modeling trees. TLS has been used in forest inventory research for about 20 years (Liang et al., 2016). Forest variables of interest have included DBH, tree height (Olofsson et al., 2014; Wang et al., 2019), and above-ground biomass (Olofsson and Holmgren, 2017; Olschovsky et al., 2016). Additional research includes modeling of stem profiles (Henning and Radtke, 2006; Liang et al., 2014; Maas et al., 2008; Mengesha et al., 2015; Olofsson and Holmgren, 2016; Raunonen et al., 2013; Thies et al., 2004) and branches (Raunonen et al., 2013). TLS can currently be used to provide estimates of DBH with an accuracy about 1 cm root mean square error (RMSE), (Olofsson and Holmgren, 2016), and interest in using TLS in commercial forest inventories has therefore increased.

ALS and TLS measurements can be combined in a straightforward

MB approach, where the traditional field measurements are replaced with the TLS measurements. However, the flight configuration for acquiring dense ALS data makes it impractical to acquire these wall-to-wall, both from a time and cost perspective. Therefore, dense ALS data is (currently) only reasonable to collect as a sample. This leads to a two-phase design of HYB inference that combines the DB and MB inferential frameworks, by considering both a first-phase probability sample (ALS strips), and a second-phase sample (TLS measurements) acquired without requirements on probabilistic principles (Gregoire et al., 2016; Holm et al., 2017; McRoberts et al., 2016; Puliti et al., 2017a; Ståhl et al., 2016, 2011). Uncertainty is quantified by the sum of the two additive components, stemming from 1) the DB sampling variability across the ALS strips, and 2) the use of a model in phase two. Using HYB inference increases complexity, but the benefits may include increased precision at a lower cost (Puliti et al., 2020, 2017a; Ståhl et al., 2016).

The overall aim of this study was to develop, demonstrate, and assess a forest inventory based on very-high-resolution laser scanning, using a two-phase sampling design under a HYB inference framework. The efficiency of the approach was assessed by comparing the estimates with empirical data for the harvested trees measured by a harvester, and by comparing the estimates with a traditional DB inventory relying on field sample measurements. Further objectives were to assess the estimation accuracy for common forest variables at the stand level: Lorey's mean height (H_L), mean diameter (D_L), stem volume (VOL), and tree species.

2. Material

2.1. Study area

The entire study area covers approximately 50,000 ha, located at 62.9° N 16.9° E in middle Sweden (Fig. 1a and b). A subset consisting of ten forest stands (Fig. 1 c, Table 1) covering 207 ha was the primary area used in this study. Additionally, a subset of trees within four long strips measuring 11 km × 80 m each systematically distributed within the study area (Fig. 1 b) was also used to train the tree species model. The study area is located in the boreal forest region and is dominated by Norway spruce (*Picea abies* (L.) H. Karst.), Scots pine (*Pinus sylvestris* L.), and birch (*Betula* spp.), with pine (50%) and spruce (44%) constituting 94% of the growing stock and birch 6%. In this study, all deciduous forest types were approximated as birch forest, since birch constitutes 86% of the deciduous forest volume in Sweden. For the stands used in this study, the average VOL was 235 m³/ha.

2.2. Field reference data

The forest in the study area is owned by SCA, a company that is the largest private forest owner in both Europe and Sweden (owning about 9% of Sweden's forests). In 2019, they carried out an extensive field inventory covering about 2% of their entire forest holding. The purpose was to obtain an accurate estimate of their entire forest holding, reference data for modeling, and evaluation data for their previous forest management. The ten stands that were used in this study were included to enable comparisons with the laser-based predictions, applying the same inventory procedure as was used for all forest stands. The ten inventoried stands were sampled with a total of 99 circular plots with a dynamic radius (from 6 to 8 m), using a probabilistic sample approach with a systematic grid that was consistent within each stand, but independent across stands. The radius was fixed for all plots within a stand but adjusted between stands to obtain an average of 15 to 20 trees per plot. This approach led to an average of 10 plots per stand (7 to 12 depending on the stand size and shape, see Table 2). To enable comparisons with the harvester data, 11 plots were eliminated because they were located outside the harvested forest area. The number of plots is described in Table 2 as N_{plots} and N_{plots_used}. The separate plot averages were used to compute the within-stand variance between the plots.

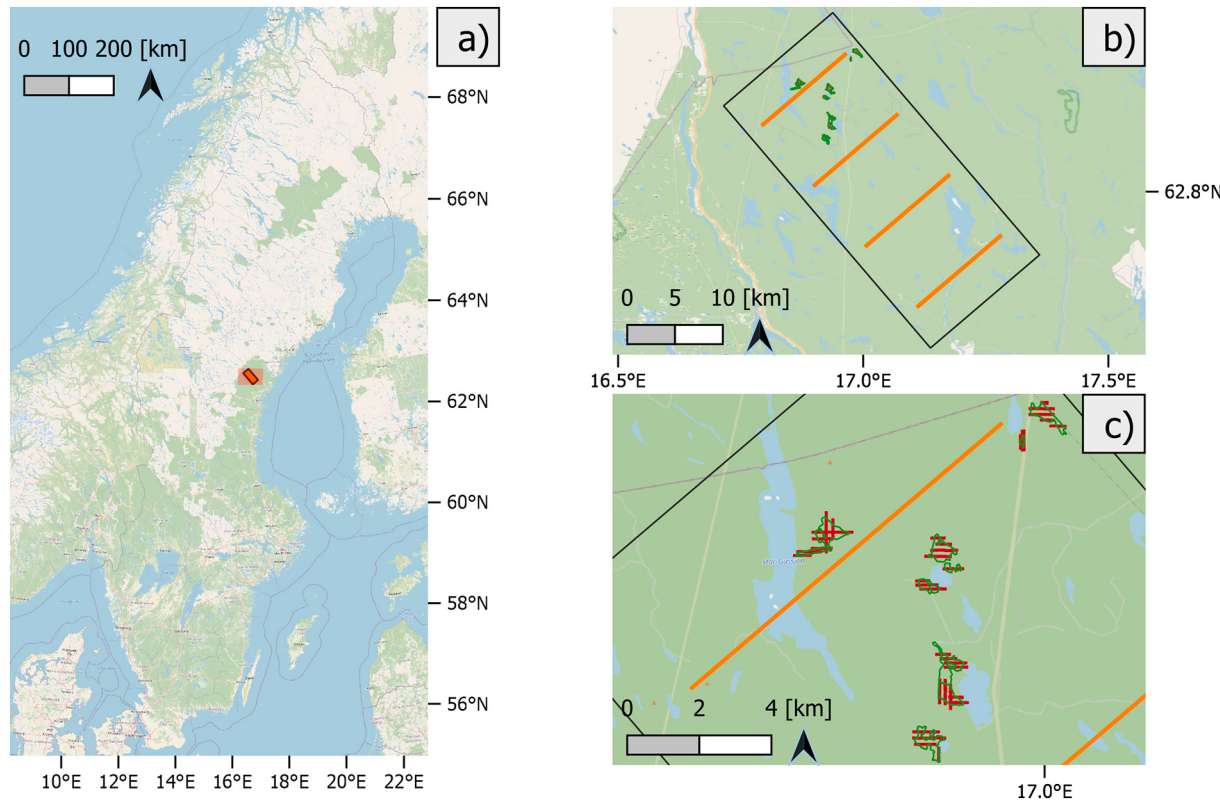


Fig. 1. a) The study area in Sweden, outlined in black with red background. b) The four long systematic flight strips (in orange) covering the study area were only used for interpretation of tree species. The shorter flight strips (in red) were covering the stands (outlined in dark green). c) The ten forest stands are outlined in dark green, and the flight strips within the stands are red. (For interpretation of the references to colour in this figure legend, the reader is referred to the web version of this article.)

Table 1
Properties of the ten forest stands used for evaluation.

Stand	Size [ha]	Mean age [yr]	Elevation [m]
S1	35.0	117	357
S2	9.65	108	384
S3	13.0	100	360
S4	36.3	100	403
S5	25.5	117	382
S6	2.25	117	350
S7	29.9	150	303
S8	23.6	108	355
S9	14.4	100	333
S10	17.9	98	341

Trees with a DBH > 4 cm were always caliper, but trees with a smaller DBH were also caliper if they were assumed to provide an economical return on investment in the future. A random subsample of trees were height-measured using a hypsometer, usually providing at least one representative tree per plot. The tree species were recorded, and the plot level VOL were computed using established equations valid for the region (Brandel, 1990). Stand-level estimates were computed as plot averages for each stand, and the tree species proportions were determined with respect to VOL. The inventoried properties for each stand are presented in Table 2.

2.3. Harvester data

Two forest harvesters were used to harvest the ten forest stands to obtain reference data that were acquired independently from the field inventory and laser data. The two harvesters were JOHN DEERE Model 1470s built in 2017 and 2018, respectively. The harvested logs were

Table 2
Properties for field inventory. The tree species are abbreviated as pine (P), spruce (S), and birch (B).

Dataset	H _L	D _L	Mean VOL (m ³ ha ⁻¹)	Trees [m ⁻¹]	N _{plots}	N _{plots used}	Tree species (% P,S,B)
S1	17.5	23.9	264	1326	10	10	42, 51, 6
S2	21.7	28.3	353	746	10	10	50, 49, 1
S3	17.4	27.2	188	1336	7	7	68, 27, 5
S4	18.7	25.5	255	915	11	11	47, 50, 3
S5	17.9	25.1	287	1130	9	8	27, 68, 5
S6	12.3	16.9	117	1037	11	7	18, 63, 18
S7	15.7	22.5	187	1028	9	7	78, 19, 3
S8	18.3	24.6	282	1326	12	12	47, 39, 15
S9	15.6	21.9	169	752	9	9	56, 32, 13
S10	18.0	25.1	226	1180	11	7	63, 27, 10

analyzed with using StanForD 2010 Harvested Production Presentation software (v1.2.20) developed by Skogforsk (Möller et al., 2011), to derive the required stem data. The harvester recorded the tree species (by visual inspection from the operator) and measured the stem diameter along the trunk at 10 cm intervals. The diameter measurements were recorded with an accuracy of 1 mm and are considered the truest available data, although the measurements are also affected by, for example, harvesting conditions (i.e., frozen conditions during winter vs. summer) (Holopainen et al., 2010; Kemmerer and Labelle, 2021; Lu et al., 2018; Miettinen et al., 2010; Siipilehto et al., 2016). The harvester also measured trunk length to the “top cut,” where the trunk is assumed

to be too small to be used. The length of the remaining (cut) part was predicted in the software using height functions and the diameter and height measurements along the trunk (Kiljunen, 2002; Möller et al., 2009). The top-cut diameter varies, since it is the leftover part of the stems that are bucked to fixed lengths, starting at the butt.

To have full control of the volumes, we used the harvesters' measurements of DBH and tree height as input to the same volume functions that were used to predict the volume from the laser and field data. All ten stands were intended to be clear-cut, but in the end, only nine of the stands were more or less completely clear-cut. Stand S3 was commercially thinned, which means that larger trees were left, with rather evenly spatially distributed trees. Due to various Swedish regulations, forest stands can rarely be entirely clear-cut. The ground conditions in some parts of the stand may be too wet to support the weight of a harvester, unstocked forest land is usually considered non-productive forest, and about 5–15% of the forest must be left as retention zones. This caused differences between the amount of forest actually harvested and the estimates of the delineated stand as obtained from the field inventory and laser scanning.

The position of the harvester cabs (Fig. 2) was recorded using a real-time kinematic global navigation satellite system (GNSS), model L5 P2 DUALGNSS, which provides sub-meter accuracy in clear-sky conditions (e.g., after harvest), and somewhat lower accuracy below standing trees. The harvester head extended 8 m from the cab at most. This would have enabled us to estimate the approximated total area covered by the harvester. However, it soon became clear that this approach was too inaccurate, and the harvested areas were therefore overflowed with a drone carrying an optical camera after the harvest. This generated orthophotos with 4 cm pixel resolution, which enabled us to delineate the harvested forest areas. To enable an adequate comparison with the laser-based predictions, only the intersecting areas were compared at the stand level. This had a large impact on the results, especially for the commercially thinned stand S3, where we therefore only included the harvested trees.

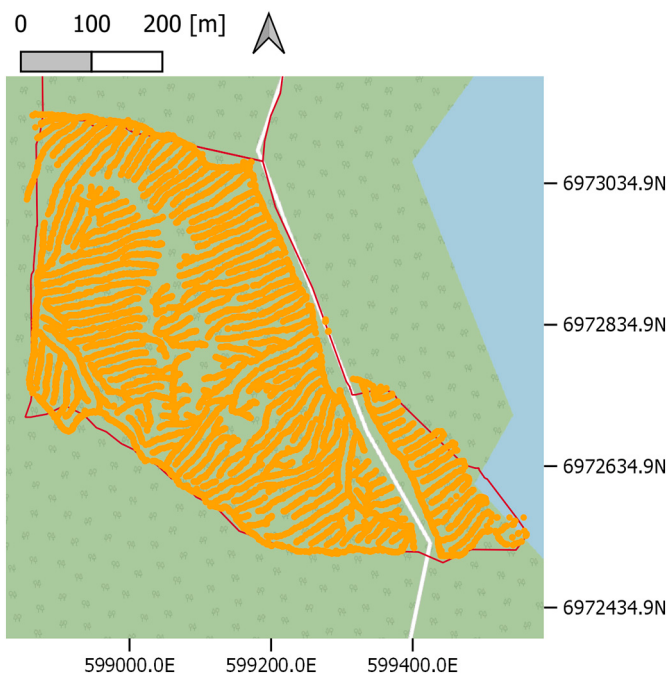


Fig. 2. The GNSS track (in orange) of the harvester for stand S8 (delineated in red). Coordinates in SWEREF99TM. (For interpretation of the references to colour in this figure legend, the reader is referred to the web version of this article.)

2.4. Airborne data

The Riegl LMS-Q680i ALS system was operated from a helicopter. The pulse repetition frequency was 400 KHz, and the scanning frequency was 135 Hz. The field of view was 60 degrees, the nominal flight speed was 20 km/h, and the altitude was 70 m above ground level. The nominal swath width was 90 m, and the nominal point density ranged from 490 points/m² to 654 points/m², with an average of 593 points/m². For the 10 forest stands, the flight trajectories were allocated to cover all field plots (41 trajectories). The laser scanning of the 10 forest stands was performed on November 3, 2019. The four long flight trajectories over the study area (outside of the stands), each with a length of approximately 11 km, were allocated systematically to obtain a good representation of the overall forest within the study area. The laser scanning of the long trajectories was performed on September 23, 2019, and it used the same equipment as the scanning of the stands.

In addition to the laser scanner, the helicopter also carried two 25 Mpixel cameras (RGB + NIR), directed in the nadir and 45° forward direction (along the flight trajectory). These images were only used to support the manual interpretation of tree species for the reference data.

2.5. Terrestrial laser scanning data

TLS was conducted at the location of the field plot centers in order to provide estimates of the diameters for a set of sample trees. The Trimble TX 8 laser scanner was set in Level 2 mode, with a point spacing of 11.3 mm at 30 m distance in a hemispherical pattern (field of view 360° × 317°). Level 2 mode takes 3 min to complete a full scan. The wavelength was 1.5 μm. A single scan setup was used, with the scanner in the center of the field plot.

3. Methods

Section 3.1 describes the inventory design, sections 3.2 and 3.3 describe the processing of single-tree data, section 3.4 describes the classification of tree species using a convolutional neural network, and section 3.5 compiles the processed data to connect the two phases. Section 3.6 then describes the statistical estimators used to estimate the target variables and precision at stand level, and 3.7 covers the evaluation of stand averages from all stands. An overview of the entire study design of the laser scanning based inventory is illustrated in Fig. 3.

3.1. Inventory design

The field inventory used sample plots that were distributed in a systematic grid within each stand (with a random reference point for each stand, see 2.3). The two-phase sampling based on laser scanning (LS) used a sampling design with ALS strips across the stands, and TLS samples within the strips, which for simplicity's sake were located at the same locations as the field plots. This generated straight ALS strips in a fixed configuration, with the strips oriented either north-south or east-west (Fig. 4). To avoid errors due to large off-nadir incidence angles, the part of the swath width used for further analysis was limited to ±25 m, corresponding to ±20°, while the entire acquired swath width was approximately 90 m. Due to financial reasons, the orientation of the flight lines were chosen such that the total flight length was minimized yet covered all field plots. In cases where complementary perpendicular strips were required, hence intersecting with the others, only one of the strips were selected for the overlapping area to maintain an unbiased method. The strips were trimmed such that only the parts within stands were used.

3.2. Single-tree processing using ALS

The ALS data were processed separately for each flight swath. The ALS heights above sea level were normalized using the terrain model

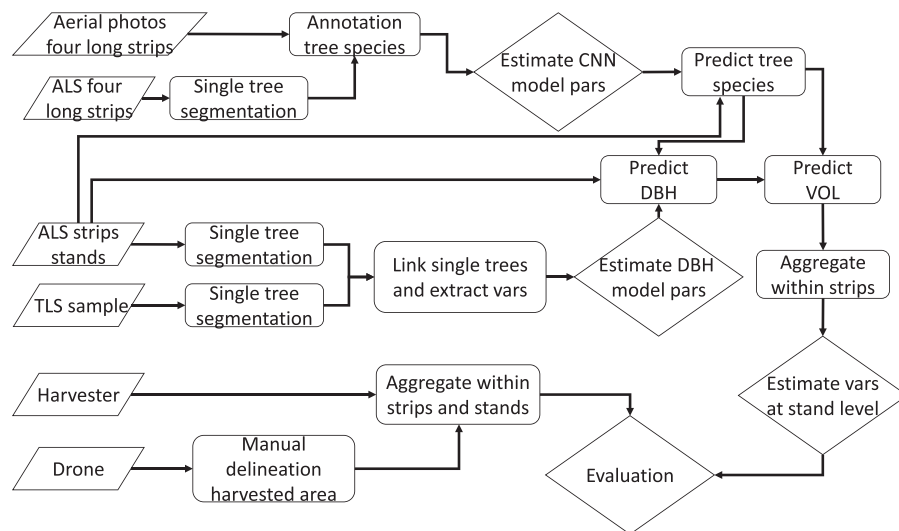


Fig. 3. Flowchart illustrating an overview of the entire laser scanning study design.

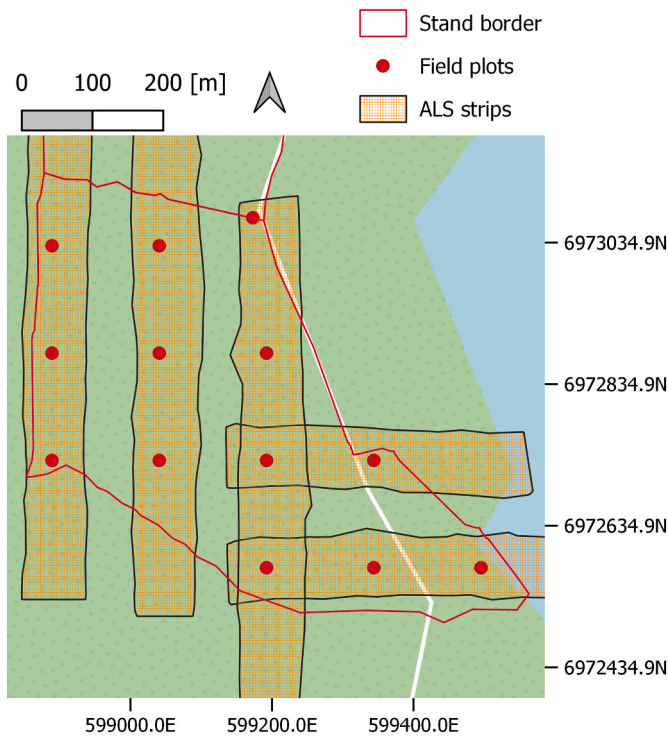


Fig. 4. The ALS sampled strips intersecting the systematically distributed field plots for stand S8. Coordinates in SWEREF99TM.

(Axelsson, 1999) to represent above-ground heights, and it was implemented in the software TerraScan (Terrasolid, Finland). For the automatic delineation of tree crowns, we used an algorithm based on density models of tree crowns (Holmgren et al., 2022). First, a canopy height model (CHM) was created for an approximate height of potential tree height positions. This was a raster with a 0.25 m raster cell size, with the maximum distance to the ground in each raster cell. The tree crown height model was set to the CHM raster cell value. Then, density models were used as templates in a watershed segmentation to identify the tree crowns. The local maxima defined the probability of the tree locations.

The density models were generated based on 78 manually delineated tree crowns. We arbitrarily selected 12 Scots pine trees, 51 Norway spruce trees, and 15 deciduous trees for the training. The trees were

normalized for height, and then we created one template for each tree species by averaging the available trees of that species.

The variables derived from the ALS data within each crown polygon included percentiles of the height distribution (10, 20, ..., 80, 90, 95, and 100), tree crown width, average height, standard deviation of heights, total number of points, height-to-crown-base, crown height, and mean intensity.

3.3. Single-tree processing using TLS

The first-phase flight strips were sampled with TLS scans at the same locations as the field plots to obtain single-tree estimates of DBH that were used to predict the DBH for all tree segments in the ALS data (further described in the section 3.5). The algorithm used to estimate the stem profiles of the trees from a 3D point cloud was that presented in Olofsson and Holmgren (2016). The algorithm first isolates the points that belong to the stems and then models the stem profiles as a number of connected, stacked cylinders. To get a continuous stem curve, the diameters along the stem were interpolated between the separate cylinders. DBH was estimated at 1.3 m above the ground using the smoothed interpolated stem curve.

The errors of the estimated stem diameters were approximately 1 cm RMSE, according to the study by Olofsson and Holmgren (2016). For an efficient computation of the large TLS dataset, the tree properties were estimated using the resources at the High Performance Computing Center North (HPC2N). Details about the algorithm are further described in Olofsson and Holmgren (2017, 2016).

3.4. Classification of tree species using a convolutional neural network

Tree species were predicted using a convolutional neural network (CNN) for the trees that were segmented in the ALS data, as an extension of the work by Wiklander (2020). As input, the 3D point cloud segments of trees were projected on to the Z axis, rotated from the XZ to the YZ plane at 0°, 30°, 60°, and 90°, providing four 2D images in total (e.g., Figs. 5 b, c, d). Testing indicated no significant improvement by adding additional projections, although processing time increased. The CNN model parameters were estimated using 2723 visually interpreted tree segments that were located within the study area but outside the stands to be estimated. In the following subsections, the steps involved to configure and train the CNN are described in detail.

3.4.1. Annotation and pre-processing of airborne data

A reference dataset was required to estimate the CNN model

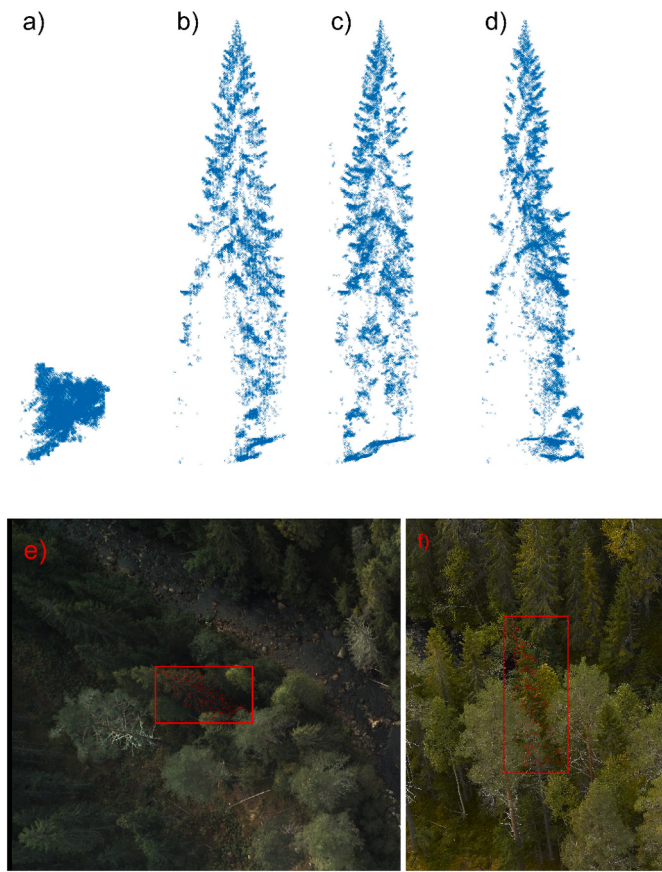


Fig. 5. a) Ortho-projection (not used in the CNN), b-d) Example of projected images of a spruce tree, used as input in the CNN, e, f) Aerial images as support for the visual interpretation of tree species.

parameters. This dataset was generated using manual visual interpretation of 2723 tree segments that had been automatically segmented in the ALS data. In addition to the laser scanner, the helicopter carried two cameras directed in the nadir and 45° forward directions (along the flight trajectory). This enabled a back-projection of the 3D point cloud for each individual tree segment to its representation in the 2D images (Figs. 5 e, f), to support the interpretation of tree species. The 2D projections of the point clouds were truncated below 0.75 m and above 32 m to restrict the image size, and the images were stored at a dimension of 153 × 699 pixels (width x height). This image size was subjectively chosen as a tradeoff between workable size, information loss, and prediction performance. The pixel values were first assigned the number of projected laser points within the pixel and then normalized by dividing by the maximum pixel value in the image. However, this “density” information did not improve the CNN classification. Therefore, images with mere zero or one values (none or at least one projected laser return) were ultimately used as input for the CNN.

Initially, 2016 trees from the four long strips were interpreted (selected as a uniform sample across species and used in Wiklander (2020)). These were clear tree segments with only a single tree in each of them, for which Wiklander showed a high classification accuracy (98%). However, the operational setting included “dirty” tree segments as well: e.g., ones that contained more than one tree or that had branches from neighboring trees overlapping the primary tree segment. This disrupted the classification, and therefore we complemented the interpretation with 707 additional random trees from the acquisition of the ten stands (so as to also match possible differences in acquisition properties) to enable an “Other” class. This helped us overcome false classifications of bad (noisy) segments, which is commonly referred to as an out-of-distribution problem (DeVries and Taylor, 2018; Gupta and Gupta,

2019; Ren et al., 2019; Zisselman and Tamar, 2020). It occurs, e.g., when a CNN is trained to classify cats and dogs and when provided an image of an airplane it returns not cat or dog but “none-of-these” as the outcome. The general aim of the manual interpretation was to obtain approximately equal classes of the tree species and include trees from all ages (although the 10 stands consisted of mainly mature forest). For our study, it did not appear necessary to put as many trees in the “Other”-class as in the species classes. However, this is a current research topic at the frontier of deep learning, which extends beyond the scope of this paper. In total, the 2723 trees (Table 3) were projected in four directions, providing a reference dataset of 10,892 labeled trees that were used for the modeling.

3.4.2. Convolutional neural network

In order to configure a suitable CNN, which was implemented in TensorFlow 2.1 and Keras 2.4.3 under Python 3.7, some initial tests were done for the commonly known networks VGG, ResNet, LeNet, and a custom Conv-Pool-Conv-Pool network. Based on the initial test performance, Resnet (He et al., 2016) and LeNet-5 (Lecun et al., 1998) were selected as base architecture for further testing. The selected ResNet architecture is known as Resnet20 v1, which provided a depth of 20 layers. For the LeNet architecture, we used Hyperas (a Keras wrapper that allows automatic numerical testing of various parameters) to sweep four suitable hyperparameters: number of channels of the convolutional layers, number of layer sequences, dropout rates, and number of neurons in the dense layers. Based on the validation accuracy, the best values for each hyperparameter were chosen and used for the final configuration of the network, which had seven layers; of these, four were convolutional and three were fully connected dense layers. The test validation showed a similar performance (93%) for both the ResNet and LeNet architectures. However, this was still a within-distribution performance metric, which in case of the LeNet architecture did not correlate with the stand-level data from the harvester. We therefore decided to use only the ResNet20 architecture as the final CNN solution, and the stand-level results are presented in the Result section. The training was carried out using a batch size of 16, since larger batches caused GPU memory problems on the Nvidia Geforce 1660 Ti graphics card. During training, 20% of the data was randomly sampled and used for validation at each iteration, and 10% of the trees ($n = 272$) were completely set aside as independent test data.

3.5. Combining single-tree properties from phase 1 (ALS) and 2 (TLS)

The practical implications of linking single-tree data from the two phases and compiling all information included co-registration and modeling of the variables. The tree properties (DBH, VOL, and tree species) were predicted and classified for the ALS trees using linear regression models, established regionally valid models (Brandel, 1990), and CNNs, respectively. The TLS provided very precise 3D reconstructions of the plots, but they were missing the global orientation. Therefore, the TLS dataset was co-registered to the ALS dataset using Olofsson et al.’s (2008) position image method. Approximately 55% of the TLS-detected trees were linked to an ALS-detected tree (Fig. 6), which, however, was sufficient to create a robust model of DBH. It was most commonly the larger, dominant trees that were successfully linked (average DBH of 19.7 cm, compared to an average DBH of 10.4 cm for

Table 3
Summary of the visually interpreted trees.

Species	Trees
Pine	691
Spruce	847
Deciduous	1022
Other	163
Total	2723

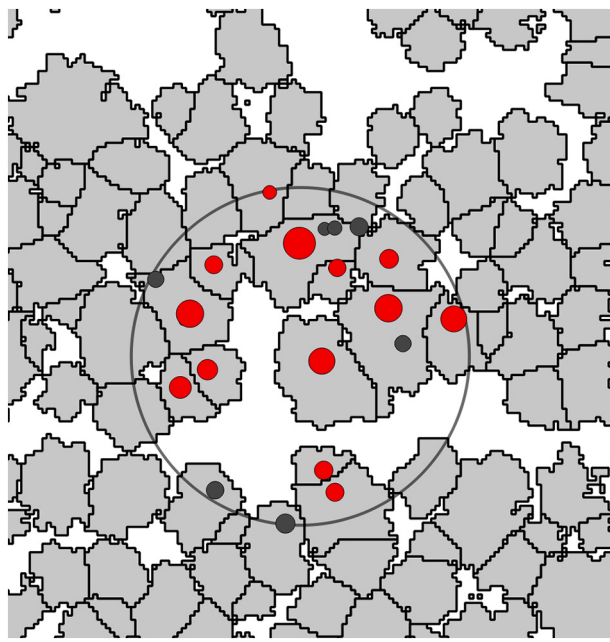


Fig. 6. Illustration of linkages at one plot location. The trees detected in the TLS data were linked to trees detected in the ALS data using a cross-correlation algorithm. The solid red circles are co-registered, linked tree locations between the two datasets. The solid gray circles are TLS-detected trees that were not linked. The size of the circles is proportional to the DBH of each tree. The large gray circle is the 10 m radius region used to search for trees to link. The light gray polygons are the tree crowns segmented in the ALS data. (For interpretation of the references to colour in this figure legend, the reader is referred to the web version of this article.)

the unlinked trees).

The matching algorithm used the tree lists from TLS and ALS, where the tree positions and tree properties were co-registered, using cross correlation of the position images. Then, the algorithm linked the trees with the smallest treetop distances. To take into account the fact that single-scan TLS data have shaded sectors that are obscured from the scanner, non-visible areas were masked from the tree position images by using only the trees that were identified in both the TLS and ALS datasets. This step provided accurately oriented trees in the global coordinates (same as ALS), with DBH estimated from TLS.

For each stand, all trees of each species that were identified in both the TLS and ALS data were used to estimate model parameters with robust multiple linear regression, using the MASS R-package and the default Huber variance estimator (Huber, 1981). The regression model was used to predict DBH on all segmented trees, and it had the form of (1),

$$\ln(\text{DBH}) = \alpha_0 + \alpha_1 X_1 + \dots + \alpha_p X_p \quad (1)$$

where the parameters $[\alpha_0, \alpha_p]$ for the p attributes $X_i, i \in [1, p]$ were the following statistical metrics computed from the ALS point clouds for the single-tree segments: height percentile 50, 80, 100, and mean intensity. If fewer than 30 trees were available for a species in a stand, the parameters were estimated from all trees from the stand, and only the height percentiles were used. Since the dependent variable DBH was transformed using the natural logarithm, a correction for logarithmic bias was applied, by adding $s^2/2$ to (1) before taking the inverse transform of the prediction, s^2 being the residual variance from (1) (Finney, 1941). VOL was predicted using established volume functions valid for northern Sweden (Brandel, 1990), with DBH, tree height, and tree species as explanatory variables.

Tree species was predicted for each tree segment using the trained CNN (see 3.4). Approximately half of the tree segments were assigned a

tree species, and the remaining were assigned “Other.” Since the tree species was required for each segment in order to use the volume functions, the “Other” segments were assigned a tree species randomly, with a probability proportional to the distribution of the successfully classified tree species.

3.6. Stand estimations

This section describes how the stand averages and precisions were estimated.

3.6.1. Design-based inference using the field samples

For the DB estimation, we assumed simple random sampling without replacement, although the variance estimator is known to be biased and conservative under systematic sampling. Assuming a sample of n field plots of the same size with equal-probability, the mean ($\hat{\mu}_{Y_{FIELD}}$) is given by the estimator (Gregoire and Valentine, 2008, p. 52):

$$\hat{\mu}_{Y_{FIELD}} = \frac{1}{n} \sum_{i=1}^n y_i \quad (2)$$

where y_i is the field reference (e.g., volume or diameter) for the i th field plot ($i = 1 \dots n$).

The DB variance of $\hat{\mu}_{Y_{FIELD}}$ was computed using the variance estimator for simple random sampling without replacement as

$$\widehat{\text{Var}}(\hat{\mu}_{Y_{FIELD}}) = \frac{1}{n} s_{Y_{FIELD}}^2 \quad (3)$$

where $s_{Y_{FIELD}}^2$ is the sample variance.

3.6.2. Two-phase hybrid inference using ALS strips

For the LS approach, the population mean ($\hat{\mu}_{Y_{LS}}$) was estimated with different estimators for the different variables. Lorey's mean height and diameter, H_L and D_L , were computed by weighing with the basal area. The stand estimates were then obtained by summation over all trees identified in the strips in each stand.

$$\hat{\mu}_{Y_{LS, \text{Lorey}}} = \frac{\sum_{j=1}^{M_a} y_j t_j}{\sum_{j=1}^{M_a} t_j} \quad (4)$$

where y_j and t_j denote the reference value (e.g., H_L) and the basal area of tree j , respectively, and M_a denotes the total number of segmented trees in all the strips in the stand.

To estimate the stand averages of VOL, we used a ratio-to-size estimator, as the size of the strips varied depending on the stand shape. As described by Kaiser (1983), the probability that a tree (whose treetop is within the strip) is sampled is proportional to the size of the strip, including in the case of random strip lengths. Following Stehman and Salzer (2000), the total volume T_k for each strip k was calculated by summing the reference values \hat{y}_j (now tree volume) predicted with the regional functions (see 3.5) for all trees M_k in the strip:

$$\hat{T}_k = \sum_{j=1}^{M_k} \hat{y}_j \quad (5)$$

Then, the mean ($\hat{\mu}_{Y_{LS,VOL}}$) was estimated as

$$\hat{\mu}_{Y_{LS,VOL}} = \frac{\sum_{k=1}^{M_c} \hat{T}_k}{\sum_{k=1}^{M_c} a_k} \quad (6)$$

where a_k denotes the total area of strip k , and M_c denotes the total number of strips in the stand.

An approximated variance (Ståhl et al., 2011) of the estimators in (4) and (6) is

$$\widehat{Var}(\widehat{\mu}_{Y_{LS}}) = s_{Y_{LS}}^2 + \sum_{d=1}^p \sum_{e=1}^p \widehat{Cov}(\widehat{\alpha}_d, \widehat{\alpha}_e) \widehat{T}'_d \widehat{T}'_e \quad (7)$$

where the first term represents variability due to the first-phase sampling and the second term represents the model error due to the uncertainty of the parameter estimates.

Following the notation in Ståhl et al. (2011), p is the number of model parameters, $\widehat{Cov}(\widehat{\alpha}_d, \widehat{\alpha}_e)$ is the estimated covariance between the model parameter estimates, and $\widehat{T}'_d \widehat{T}'_e$ are the estimated average values of the first order partial derivatives of the function used to predict the target variable. In this study, the estimation of uncertainty due to the model parameters was only relevant (non-zero) for the estimation of DBH. Height was a pure laser measurement in the first phase, without any function involved, and for the estimation of VOL, we used the same regression function for both the harvester reference values and those predicted from the field data and LS data. This means that the possible effect of uncertainty in the volume model parameters will affect both the reference and predicted values in a like manner and cancel out.

The first-phase sampling variability can be estimated as corresponding to Stehman and Salzer (2000, Eq. 3) or Gregoire and Valentine (2008, Eq. 6.14):

$$s_{Y_{LS}}^2 = \left(1 - \frac{a}{A}\right) \frac{\sum_{k=1}^{M_c} (\widehat{T}_k - \widehat{\mu}_{Y_{LS}} a_k)^2}{M_c a^2 (M_c - 1)} \quad (8)$$

where a represents the area covered by the strips, A represent the total area of the population (stand), and \bar{a} is the mean strip area.

3.7. Evaluation strategy

We quantified the mean accuracy of the respective inventory approach via the metrics root-mean-square-error (RMSE) and bias, when compared with stand averages in the reference data (generally measured by the harvester). Additionally, we estimated the mean precision using the standard error (SE). The metrics were also expressed as percentages relative to the mean estimates.

To provide an estimate of mean bias, the estimated stand means ($\widehat{\mu}_{Y_i}$) from field data or LS data were compared with the reference values μ_{Y_i} from the harvester, and the mean population bias for the M_d stands was estimated as.

$$\widehat{B} = \frac{1}{M_d} \sum_{i=1}^{M_d} (\widehat{\mu}_{Y_i} - \mu_{Y_i}) \quad (9)$$

The HYB inference framework is not unbiased since it relies on a correctly specified model in the second phase. Since the stands were completely harvested and measured, we could empirically estimate the model bias for the HYB inference in the regions covered by both ALS and the harvester. This was accomplished by using Eq. 9, but limiting the comparison to only those trees that were harvested within the flight strips, hence eliminating the sample variance component. This gave an empirical estimate of the mean systematic deviation using HYB inference. Since the field plots were small, with inaccurate positions (5–10 m accuracy), it was not meaningful trying to correspondingly estimate the bias for those.

The RMSE was estimated as

$$\widehat{RMSE} = \sqrt{\frac{1}{M_d} \sum_{i=1}^{M_d} (\widehat{\mu}_{Y_i} - \mu_{Y_i})^2} \quad (10)$$

using the same notations as before.

The SE was calculated as the square root of the variance:

$$\widehat{SE} = \sqrt{\widehat{Var}(\widehat{\mu}_Y)} \quad (11)$$

The mean SE for all M_d stands was estimated as

$$\overline{\widehat{SE}} = \frac{1}{M_d} \sum_{i=1}^{M_d} \widehat{SE} \quad (12)$$

4. Results

4.1. Stand-level accuracy

The ALS-based stand estimates were generally more accurate than the field inventoried estimates (Table 4 and Figs. 7). In many applications, VOL is considered the most important variable, due to its strong relation with forest value, but also due to the amount of stored carbon. When using LS, the uncertainty expressed as mean bias and RMSE of VOL were rather low (2.5% and 7.2%, respectively, Table 4). The positive bias indicates that possibly missed trees would be small and suppressed and did not have any significant impact on the overall VOL estimates. The field-based VOL estimates were also positively biased (1.8%), but with a higher RMSE (17%), which can also be noticed in the larger spread about the 1:1 line in Fig. 7 b.

The LS-based estimates of H_L were showing a small negative bias (−3.3%) and lower RMSE (4.6%) than those obtained from the field inventory (−7.2% bias and 8.3% RMSE). The height estimates from ALS were obtained as direct height measurements in the first phase using the dense ALS data. Thus, it is likely that some laser points should reflect the treetops accurately. The systematic underestimation of height could therefore be due to inaccurate measurements of the harvester, which varies with the cutting height of the stump and only measures the tree to the last cut on the trunk. This means that the last 2–3 m are never measured but only estimated, which could be one potential cause for this bias.

The results, in relative terms, were similar for the estimates of D_L , where bias and RMSE were −3.5% and 6.0%, respectively, for the LS data and −4.3% and 7.7%, respectively, for the field samples.

The empirically estimated model bias of the HYB inference framework indicated the lowest bias (in relative terms) for the volume estimates, 4.00 m³/ha (1.68%). The corresponding bias for H_L and D_L was −0.720 m (−3.74%), and −11.2 mm (−4.31%), respectively. A low bias is important since the HYB inferential framework is not unbiased per se. A small misspecification of the model could accumulate and cause significant errors when aggregated.

When the ALS-based estimates were evaluated using the field samples as reference (Table 5), the RMSE of VOL (Fig. 8) increased from 7.2% to 18.6%, while the bias decreased slightly from 2.47% to 0.68%. The RMSE of H_L increased correspondingly, from 4.63% to 8.94%, while the RMSE of D_L is the only variable that resulted in a lower RMSE, dropping from 5.99% to 4.09%. This indicates that using field data as a reference when evaluating forest RS estimates can constitute a significant error source that inflates the reported RS accuracy, especially when the field data are based on a sample. This has been noted earlier by Persson and Ståhl (2020).

4.2. Precision of inferential frameworks

The precisions of the two inventory systems (field and LS, under the DB or HYB inferential frameworks) are presented in Tables 6, 7, and 8.

Table 4

Accuracy for mean stand predictions based on laser scanning and field plots, respectively.

Dataset	Variable	Bias	RMSE
ALS vs. Harvester	VOL (m ³ /ha)	5.83 (2.47%)	17.1 (7.24%)
Field vs. Harvester	VOL (m ³ /ha)	4.20 (1.78%)	40.7 (17.2%)
ALS vs. Harvester	H_L (m)	−0.62 (−3.26%)	0.88 (4.63%)
Field vs. Harvester	H_L (m)	−1.37 (−7.18%)	1.59 (8.30%)
ALS vs. Harvester	D_L (mm)	−8.94 (−3.46%)	15.5 (5.99%)
Field vs. Harvester	D_L (mm)	−11.2 (−4.32%)	19.8 (7.65%)

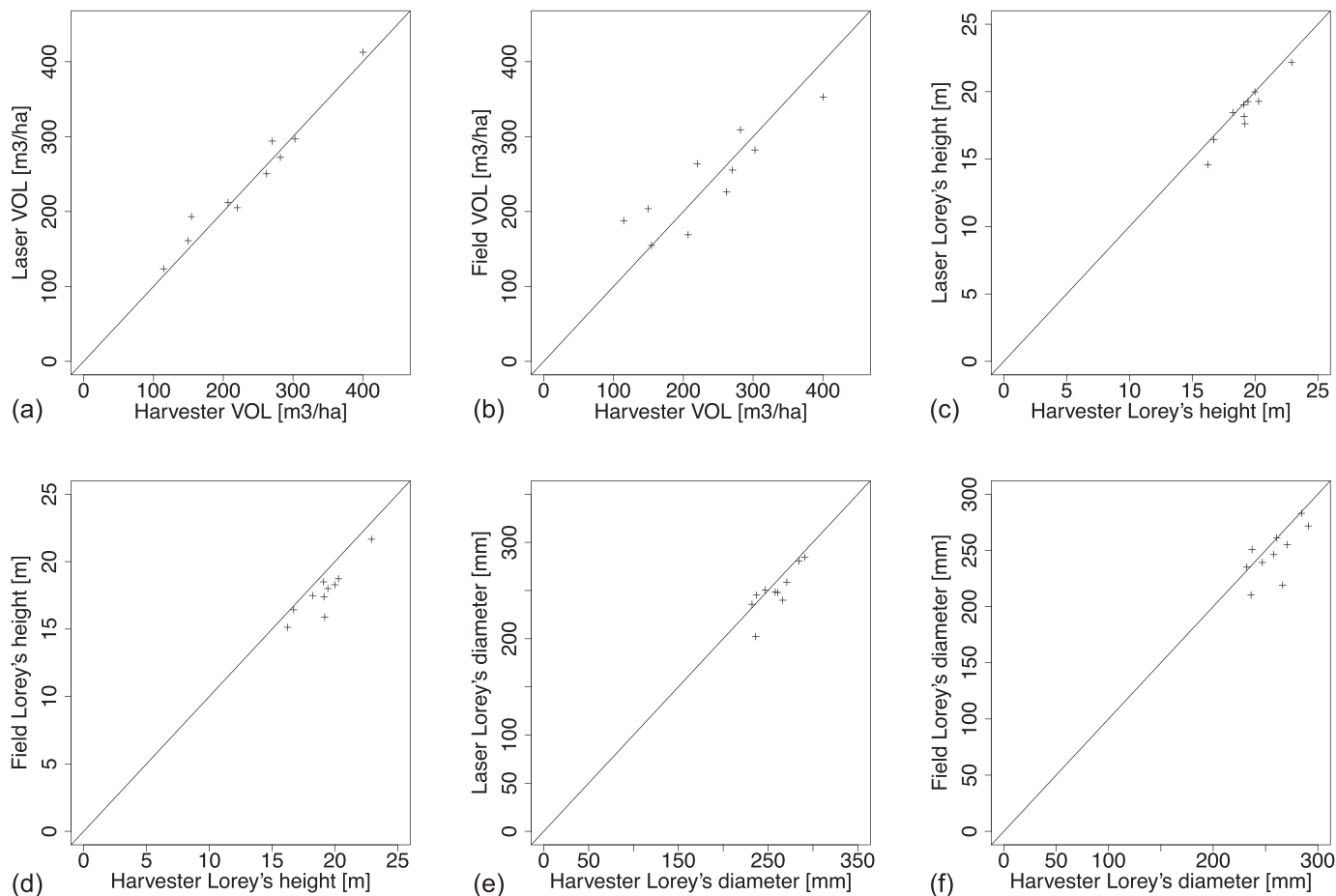


Fig. 7. Scatterplots of estimates from either laser or field data vs. harvester. a) ALS vs harvester, VOL. b) Field vs. harvester, VOL. c) ALS vs. harvester, H_L. d) Field vs. harvester, H_L. e) ALS vs. harvester, D_L. f) Field vs. harvester, D_L.

Table 5
Accuracy for mean stand predictions when compared with field data.

Dataset	Variable	Bias	RMSE
ALS vs. Field	VOL (m ³ /ha)	1.63 (0.68%)	44.7 (18.6%)
ALS vs. Field	H _L (m)	1.37 (7.74%)	1.59 (8.94%)
ALS vs. Field	D _L (mm)	2.23 (0.90%)	10.1 (4.09%)

Table 6
Mean SE from all stands for the inventory methods. Bias was estimated from the harvested trees within the flight strips.

Dataset	Inference	Variable	\widehat{SE}
LS	HYB	VOL (m ³ /ha)	15.6 (6.62%)
Field	DB	VOL (m ³ /ha)	40.3 (17.0%)
LS	HYB	H _L (m)	0.657 (3.43%)
Field	DB	H _L (m)	1.24 (6.47%)
LS	HYB	D _L (mm)	15.5 (6.02%)
Field	DB	D _L (mm)	20.6 (7.97%)

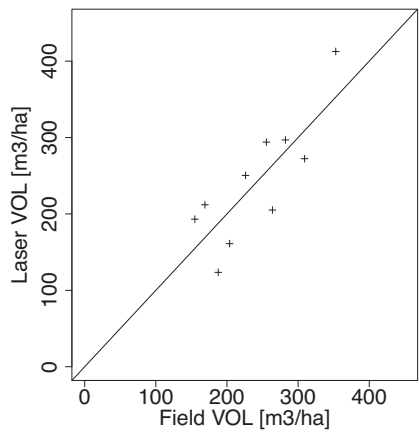


Fig. 8. Scatterplot of laser vs. field data estimates, VOL.

Table 7
Precision of VOL estimates (m³/ha) expressed as the SE for each stand. Variability due to uncertainty in the model parameters were not possible to estimate for LS VOL, and therefore these values only contain the sample variances. Stand S6 was completely covered by the ALS strips and therefore the sampling error was zero.

Stand	\widehat{SE}_{Field}	\widehat{SE}_{LS}
S1	34.0 (15.4%)	17.7 (8.06%)
S2	52.7 (13.2%)	23.4 (5.85%)
S3	38.5 (33.6%)	8.49 (7.41%)
S4	25.7 (9.53%)	15.6 (5.77%)
S5	68.7 (24.4%)	13.0 (4.61%)
S6	31.1 (20.2%)	0
S7	36.7 (24.6%)	15.3 (10.2%)
S8	38.5 (12.7%)	15.2 (5.02%)
S9	29.5 (14.3%)	15.3 (7.42%)
S10	27.4 (10.4%)	22.0 (8.39%)

Table 8

Precision of DBH estimates (mm) expressed as SE for each stand. Variability due to uncertainty in the model parameters is given as a percentage of the total variance. Stand S6 was completely covered with the ALS strips, and therefore the sampling error is 0, and the SE consisted only of the model parameter uncertainty.

Stand	\widehat{SE}_{Field}	\widehat{SE}_{LS}	Variance proportion model error
S1	20.3 (9.22%)	20.9 (9.52%)	12.9%
S2	12.3 (3.07%)	8.65 (2.16%)	46.5%
S3	32.2 (28.1%)	29.8 (26.0%)	10.8%
S4	10.0 (3.70%)	12.1 (4.47%)	20.0%
S5	19.0 (6.76%)	18.1 (6.41%)	29.9%
S6	21.4 (13.9%)	5.22 (3.38%)	100%
S7	12.9 (8.62%)	15.8 (10.6%)	37.7%
S8	13.7 (4.54%)	9.40 (3.10%)	62.7%
S9	32.3 (15.6%)	11.5 (5.55%)	91.2%
S10	17.8 (6.80%)	6.96 (2.65%)	74.5%

Using LS, the mean SE for VOL was 6.7%, and with the field samples, the mean SE was 17% (Table 6). The SEs for the stand VOL estimates were consistently 23 m³/ha or lower, which corresponded to a SE of 10.2% at most (Table 7). The same VOL model was used for both the LS estimates and the harvester references, and the model error component in (7) was therefore cancelling out to zero. The SEs for height were 3.4% and 6.4% when estimated from LS and field data, respectively. The precision of the LS diameter estimates are interesting since they are the only estimates completely involving all parts of the HYB inferential framework. \widehat{SE}_{LS} therefore contains both the sampling variance and the model error (7). The variance proportion of the total variance due to uncertainty in the model parameters is listed in the rightmost column. It varied between 10.8% and 100%; the extreme case (100%) appeared for stand S6, which was entirely covered by the flight strips and the only variance component was therefore due to the use of a model.

4.3. Tree species

The tree species could be classified for about half of the trees, and the remaining trees were assigned to the “Other” class. This seemed to be sufficient for accurately estimating the proportions at the stand level. In Fig. 9, the stand averages per tree species are illustrated. The corresponding quantified values are listed in Table 9. In relative terms, the

Table 9

Evaluation of VOL per tree species at the stand level.

Dataset	Method	Variable	Bias (m ³ /ha)	RMSE (m ³ /ha)
Pine	LS	VOL (m ³ /ha)	-1.20 (-1.06%)	10.6 (9.28%)
Spruce	LS	VOL (m ³ /ha)	1.44 (1.34%)	15.4 (14.3%)
Birch	LS	VOL (m ³ /ha)	-5.59 (37.2%)	9.42 (62.7%)
Pine	Field	VOL (m ³ /ha)	2.67 (2.34%)	40.9 (36.0%)
Spruce	Field	VOL (m ³ /ha)	-4.03 (-3.74%)	27.4 (25.5%)
Birch	Field	VOL (m ³ /ha)	1.58 (10.5%)	10.3 (68.3%)

RMSE and bias were low for pine and spruce (9–14% RMSE) and higher for birch (63% RMSE). The apparently large errors for birch trees are somewhat misleading, since their proportions of the overall stand VOL were low. The corresponding accuracies, when estimated from field plots, showed a similar order of bias, while the RMSEs were higher (26% to 68%).

5. Discussion

In this study, a two-phase sampling approach relying on HYB inference was empirically validated for an inventory of ten forest stands. This study found that strip samples of dense ALS data combined with TLS samples were suitable for generating accurate stand-estimates of VOL, H_L, D_L and tree species. It furthermore found that this inventory method decreased the uncertainties of estimates at the stand level significantly compared to traditional field sampling methods. The RMSE of the estimated VOL decreased more than 50% compared to the field inventory. Furthermore, it was found that when the estimates based on ALS were compared to the field estimates, the apparent ALS accuracy was heavily affected and limited by the accuracy of the field estimates. The dense laser data enabled us to work at the single-tree level. The use of a harvester to collect validation data provided full control of all harvested trees, which contributed to the good results. Furthermore, the proposed method is not dependent on laborious manual field measurements.

Estimates of VOL from single-tree methods have previously been reported to have an accuracy in the range of 13% to 17% in Scandinavian forest conditions, while accuracy for H_L and D_L has commonly been reported to be in the range of 8% to 10% and 16% to 20%, respectively (Breidenbach et al., 2010; Peuhkurinen et al., 2011). In this context, our results appear promising. Two factors contributing to the improved results were the dense LS data and the more accurate validation data, due

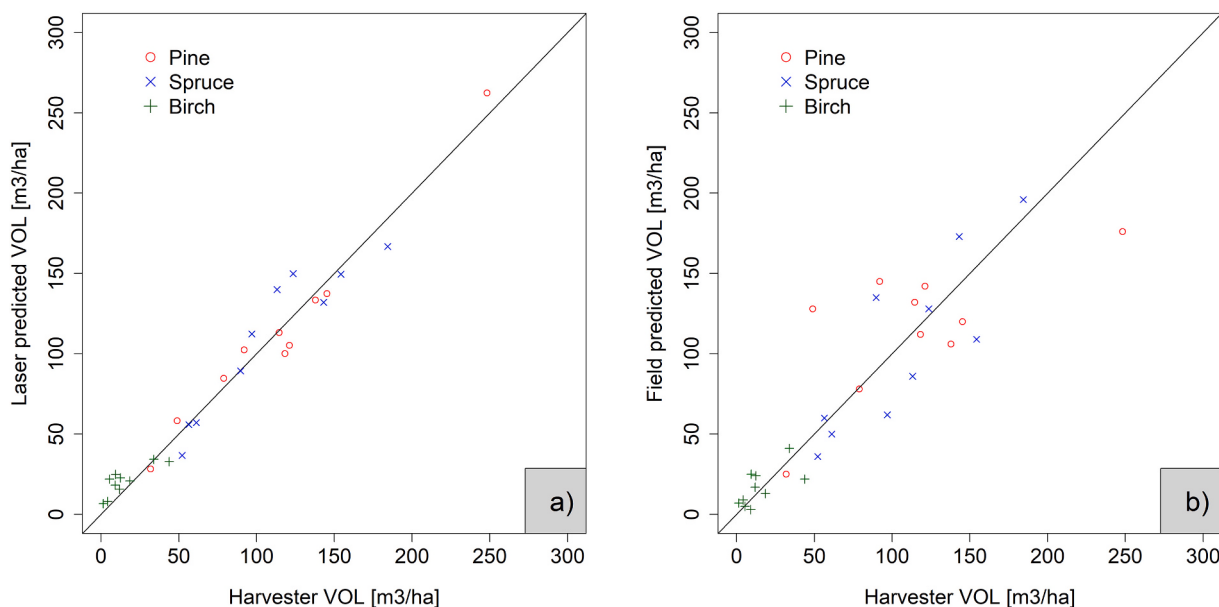


Fig. 9. a) The laser-predicted VOL per tree species at the stand level. b) The field-estimated VOL per tree species at the stand level.

to the use of harvester measurements. The harvester enabled a complete inventory of all trees with accurate DBH and height measurements, although the limited positional accuracy of the harvester head required manual delineation of the harvested areas. Single-tree methods may be prone to systematic errors if not handled carefully. Our approach was based on sample trees from each stand, with DBH estimated from TLS being linked to dense ALS data. The small mean bias of all variables at validation indicates that the use of sample trees from each stand is an option to reduce model-related systematic errors. For operational settings, sample trees from all stands are not feasible, and the impact of using generic models valid for an entire region should be further investigated.

Accurate estimates of tree species proportions or single-tree classifications based on RS have previously been considered too inaccurate to be useful for Swedish forestry practitioners. The tree-level predictions and tree species identification made it possible to predict tree-specific stem volumes with low estimation errors in forest stands with a mixture of tree species as well (Fig. 9, Table 9, primarily coniferous species). In the context of forest inventories in Scandinavia, the classification of tree species is most important in terms of volume and aggregated at the stand level. The laser-based estimates were considerably more accurate than those based on field samples. This is encouraging, since tree species has long been reported to be one of the most important variables to map, although efficient methods to do so have been limited (Kangas et al., 2018). CNNs have been increasingly used for classifying tree species, although practical challenges remain, including requirements for sufficient reference data (we used 2723 trees projected from four directions, corresponding to 10,892 sample trees) and the desired repeatability in research applications (deep learning is not deterministic in its nature (Morin and Willets, 2020)).

One limitation with the harvester data in the current study was positioning, which was only provided for the harvester cab and not for the harvester head (and hence single trees). This caused uncertainties related to delineating the harvested area, which affected the area-based estimates (e.g., VOL/ha). Visual post-interpretation of drone images was probably less accurate than what could be obtained from accurate GNSS sensors mounted on the harvester head. Furthermore, retention trees and other trees that were not harvested could have been automatically filtered out. Accurate positioning of the harvester head requires accurate sensors of the boom tip position combined with accurate GNSS positioning of the cabin. With this, a more thorough study of the accuracy of the cab position and corresponding single-tree locations could be achieved (Hauglin et al., 2017, 2018; Noordermeer et al., 2021).

Different types of multi-phase sampling methods have been proposed over the years, seeking to balance accuracy and costs. When wall-to-wall data are available, (which can be obtained at higher quality for smaller areas), MB approaches are typically preferred. For example, Hauglin et al. (2014) predicted Norway spruce crown biomass using ALS data trained with reference data from a TLS. They reported a slight improvement (32% accuracy) compared to training the model with field plots (35%). Multi-phase sampling is, due to the nature of sampling, therefore most suited for large areas, where wall-to-wall auxiliary data are not feasible. An ALS and field-based two-phase sampling at the regional level in Norway was demonstrated by Gobakken et al. (2012). They investigated a MB and a model-assisted approach, finding that the MB provided the best results, with an RMSE between 15% and 45% of above-ground biomass for different biomass classes. They also reported that the model error, expressed as percentage of the total variance, ranged between 11% and 78% using the MB approach. Puliti et al. (2017a, 2017b) have also proposed various combinations of one- and two-phase approaches, combining field plots with auxiliary data from drones or ALS, both on smaller forest properties and at larger scales. They demonstrated how a HYB inference approach with a sample of auxiliary drone data could be more than four times as efficient compared to using a traditional probability field sample when used for a large-scale inventory. The RMSE of 44 m³/ha for the drone HYB inference approach

corresponded to about 17% of the mean volume estimated from field samples.

The combined use of ALS and TLS has also been demonstrated in previous studies, although rarely in a combined multi-phase approach as we propose. Lindberg et al. (2012) used a method for automatic linking of trees detected in TLS data with trees detected in ALS data, and then used the TLS data as reference data to estimate parameters for regression models. The tree-level regression models were used for predictions of DBH using metrics from ALS data, and the predictions were nearly as accurate as when using reference data consisting of manual measurements. Other studies that combined ALS and TLS include Kankare et al. (2015), who investigated how TLS and ALS data could be combined to estimate diameter distributions in a Finnish forest. The overall RMSE was 37 mm, and they reported lower accuracies for denser forests. Bazezew et al. (2018) investigated how ALS and TLS could be used to delineate trees and estimate DBH, tree height, and above-ground biomass in tropical forests in Malaysia. Giannetti et al. (2018) assessed the potential of combining ALS and TLS data in a complex mixed Mediterranean forest to estimate different tree attributes. They reported an RMSE for tree diameter estimates of 11 to 13 mm when using point clouds from TLS or handheld LS. They did not combine the ALS and TLS data to predict TLS metrics on trees based only on ALS, and their results are therefore not comparable to ours. The performance and conditions have changed due to technical developments of the sensors since the earliest studies that were carried out in this field, which compared and assessed tree estimates from ALS and TLS (Hilker et al., 2010; Hosoi et al., 2010; Lovell et al., 2003) or LS with field measurements (Wezyk et al., 2007). Current research may suggest an improved design for the second phase in the future, e.g., by replacing the TLS plots with mobile laser scanning transects (Forsman et al., 2016; Hyppä et al., 2020; Liu et al., 2021).

We did not evaluate stocking (number of trees/ha) specifically in this study, but since VOL was estimated as a summation of single trees, our findings nevertheless indicate that most tree segments were correctly captured. Future studies should investigate to what degree suppressed trees may also be identified in the dense ALS data. However, manual field measurements with known tree positions are needed for validation of tree detection in order to derive both commission and omission errors. The stocking was high in the ten validation stands, with >1000 trees/ha in seven of the stands, despite the maturity of the forests, which can be explained by an abundance of trees in lower canopy layers. In this study, we only used TLS with one viewpoint for each field plot, which was efficient for the collection of sample trees in various forest types. However, the TLS procedure used resulted in sectors that were screened from the scanner's viewpoint. Thus, the stem number for the data used for training remained unknown, which made it unfeasible to apply a semi-individual approach, as proposed by Breidenbach et al., 2010. In future work, multi-scan TLS or mobile laser scanning could be used in order to cover all parts of the plots used in the training phase.

The precision of the VOL estimates using LS was generally high, with relative values of 10% and lower (Table 7). The error related to the estimated variance contribution due to using a TLS-based model was compared with the estimated total variance for the DBH estimates, where the latter also included sampling errors. The proportion accounted for by model errors ranged between 10.8% and 100%, which is a large variation, but which is in line with or a bit lower than previous research in a similar context (McRoberts et al., 2016; Puliti et al., 2017a). Often, the model proportion decreases as the study area increases (Breidenbach et al., 2014; Holm et al., 2017; Ståhl et al., 2014).

The deep learning model for classifying tree species was first trained on interpreted trees only from the four longer strips within the study area (within a previous work (Wiklander, 2020)). However, these trees were noise-free and often not representative of the applied cases. Furthermore, these strips were acquired six weeks prior to when the stands were laser scanned. Therefore, this model performed poorly when applied to the strips covering the stands (which were investigated in the

current study). Thus, a set of additional trees (both clean and noisy, but located outside of the investigated stands) were interpreted and added to the modeling from the latter acquisition (which covered the stands). This stabilized the model's performance considerably. It is important to further investigate the generalization of deep learning models in future studies since they require larger training datasets, and the same model would therefore preferably be useful and correct in a wider context.

The ten forest stands were all relatively homogenous in terms of age and forest type, and it would be beneficial in future research to include a wider range of forest. Nevertheless, older forests that are ready to be harvested are the most important for foresters to be able to estimate accurately, and it was not possible to obtain harvested tree data from other forest age classes.

The complexity of the method proposed in this study may hinder operational applications. However, the annotation of training data for the tree species can be performed in many ways, and the method is suitable to do with a harvester as soon as accurate positioning of the harvester head becomes available. It may also be re-used in other studies, i.e., new applications could build upon our annotated dataset. Furthermore, if the tree species is not important, this part of the procedure can be entirely left out. The linking of trees across the two phases (ALS and TLS) is necessary for the demonstrated approach, but using regional models for the height/diameter relationship could possibly eliminate this need. Regional models may be sufficient in many cases, and this would further reduce costs and manual work.

In this work, we compared a new approach, which is based on automatic measurements of trees, with manual field measurements from an operational forest inventory. The manual field inventory is currently used by forestry companies in Sweden to sample a representative subset of all their forest stands in order to have data to support strategic decisions. The same approach can also be used in other kinds of inventories: for example, national forest inventories. Several variables cannot be estimated from RS data. However, variables correlated with canopy structure could be estimated with higher efficiency in our study using a two-phase sampling approach.

6. Conclusions

This study demonstrates a complete forest inventory system, suitable for larger scales, which is based only on very-high-resolution laser scanning. It was used to estimate forest volume, diameter, and height and to classify tree species. Six conclusions can be drawn from the study. First, the dense LS-based inventory provided more accurate stand estimates than field-based and past laser-based demonstrations. Second, the combined use of LS and deep learning was successful in determining tree species. Third, although deep learning provided an accurate determination of tree species, it was necessary to include sample trees (with noise) from the acquisition of the target population to enable a successful transferability. One note is that the non-deterministic nature of deep learning made it difficult to troubleshoot the deep learning-based species classifications. Fourth, the use of a two-phase design with HYB inference (with sample trees whose diameter was measured with TLS) appears feasible for this type of forest inventory. Fifth, access to single trees measured by a harvester increased the quality of the validation data and reduced the sampling-related uncertainty. The sixth and last conclusion is that field-measured plot data were not sufficiently accurate to validate the LS-based estimates generated in this study.

The demonstrated LS-based inventory appears feasible for generating estimates at the stand level and furthermore shows potential for generating estimates at the regional or larger scales. The need for sample trees and local tree species models should be further investigated to address suitability at other scales.

Credit author statement

Methodology: HJP, JH. Investigation: HJP, JH. Validation: HJP.

Formal analysis: HJP. Software: all authors; Resources: all authors. Data Curation: all authors. Writing - original draft: HJP. Writing - review & editing: all authors.

Declaration of Competing Interest

The authors declare no conflicts of interest.

Acknowledgments

The work in this study was funded by the Bo Rydin Foundation for Scientific Research (award no F19/17) and Mistra Digital Forest (DIA 2017/14 #6). The authors wish to thank Erik Willén and Jon Söderberg at Skogforsk for support in analyzing the harvester data logs, and the anonymous reviewers whose careful review of the manuscript led to substantial improvements. The High Performance Computing Center North (HPC2N) is acknowledged for providing data resources related to the TLS computations.

References

- Axelsson, P., 1999. Processing of laser scanner data – algorithms and applications. *ISPRS J. Photogramm. Remote Sens.* 54, 138–147.
- Bazezew, M.N., Hussin, Y.A., Kloosterman, E.H., 2018. Integrating airborne LiDAR and terrestrial laser scanner forest parameters for accurate above-ground biomass/carbon estimation in Ayer Hitam tropical forest, Malaysia. *Int. J. Appl. Earth Obs. Geoinf.* 73, 638–652. <https://doi.org/10.1016/j.jag.2018.07.026>.
- Brändel, G., 1990. *Volumfunktioner för Enskilda Träd : Tall, Gran Och Björk = Volume Functions for Individual Trees : Scots Pine (*Pinus sylvestris*), Norway Spruce (*Picea abies*) and Birch (*Betula pendula* & *Betula pubescens*)*. Swedish University of Agricultural Sciences, Garpenberg.
- Breidenbach, J., Næsset, E., Lien, V., Gobakken, T., Solberg, S., 2010. Prediction of species specific forest inventory attributes using a nonparametric semi-individual tree crown approach based on fused airborne laser scanning and multispectral data. *Remote Sens. Environ.* 114, 911–924. <https://doi.org/10.1016/j.rse.2009.12.004>.
- Breidenbach, J., Anton-Fernandez, C., Petersson, H., McRoberts, R.E., Astrup, R., 2014. Quantifying the model-related variability of biomass stock and change estimates in the Norwegian national forest inventory. *For. Sci.* 60, 25–33. <https://doi.org/10.5849/forsci.12-137>.
- Burt, A., Disney, M., Calders, K., 2019. Extracting individual trees from lidar point clouds using treeseg. *Methods Ecol. Evol.* 10, 438–445. <https://doi.org/10.1111/2041-210X.13121>.
- Dalponte, M., Bruzzone, L., Gianelle, D., 2011. A system for the estimation of single-tree stem diameter and volume using multireturn LiDAR data. *IEEE Trans. Geosci. Remote Sens.* 49, 2479–2490. <https://doi.org/10.1109/TGRS.2011.2107744>.
- Dalponte, M., Ørka, H.O., Ene, L.T., Gobakken, T., Næsset, E., 2014. Tree crown delineation and tree species classification in boreal forests using hyperspectral and ALS data. *Remote Sens. Environ.* 140, 306–317. <https://doi.org/10.1016/j.rse.2013.09.006>.
- Dalponte, M., Frizzera, L., Gianelle, D., 2019. Individual tree crown delineation and tree species classification with hyperspectral and LiDAR data. *PeerJ* 6. <https://doi.org/10.7717/peerj.6227>.
- DeVries, T., Taylor, G.W., 2018. Learning confidence for out-of-distribution detection in neural networks. *arXiv:1802.04865 [stat.ML]* 1–12. <https://arxiv.org/abs/1802.04865>.
- Finney, D.J., 1941. On the distribution of a variate whose logarithm is normally distributed. *J. R. Stat. Soc. Ser. B* 7, 155–161.
- Forsman, M., Holmgren, J., Olofsson, K., 2016. Tree stem diameter estimation from Mobile laser scanning using line-wise intensity-based clustering. *Forests* 7, 32. <https://doi.org/10.3390/F7090206>.
- Frair, J.L., Fieberg, J., Hebblewhite, M., Cagnacci, F., DeCesare, N.J., Pedrotti, L., 2010. Resolving issues of imprecision and habitat-biased locations in ecological analyses using GPS telemetry data. *Philos. Trans. R. Soc. B Biol. Sci.* 365, 2187–2200. <https://doi.org/10.1098/rstb.2010.0084>.
- Gianetti, F., Puletti, N., Quatrini, V., Travagliini, D., Bottalico, F., Corona, P., Chirici, G., 2018. Integrating terrestrial and airborne laser scanning for the assessment of single-tree attributes in Mediterranean forest stands. *Eur. J. Remote Sens.* 51, 795–807. <https://doi.org/10.1080/22797254.2018.1482733>.
- Gobakken, T., Næsset, E., Nelson, R., Bollandsås, O.M., Gregoire, T.G., Ståhl, G., Holm, S., Ørka, H.O., Astrup, R., 2012. Estimating biomass in Hedmark County, Norway using national forest inventory field plots and airborne laser scanning. *Remote Sens. Environ.* 123, 443–456. <https://doi.org/10.1016/j.rse.2012.01.025>.
- Gregoire, T.G., 1998. Design-based and model-based inference in survey sampling: appreciating the difference. *Can. J. For. Res.* 28, 1429–1447. <https://doi.org/10.1139/x98-166>.
- Gregoire, T.G., Valentine, H.T., 2008. *Sampling Strategies for Natural Resources and the Environment*. Chapman and Hall, Boca Raton, FL, USA.
- Gregoire, T.G., Næsset, E., McRoberts, R.E., Ståhl, G., Andersen, H.E., Gobakken, T., Ene, L., Nelson, R., 2016. Statistical rigor in LiDAR-assisted estimation of

- aboveground forest biomass. *Remote Sens. Environ.* 173, 98–108. <https://doi.org/10.1016/j.rse.2015.11.012>.
- Gupta, S., Gupta, A., 2019. Dealing with noise problem in machine learning data-sets: a systematic review. *Proc. Comput. Sci.* 161, 466–474. <https://doi.org/10.1016/j.procs.2019.11.146>.
- Hamraz, H., Jacobs, N.B., Contreras, M.A., Clark, C.H., 2019. Deep learning for conifer/deciduous classification of airborne LiDAR 3D point clouds representing individual trees. *ISPRS J. Photogramm. Remote Sens.* 158, 219–230. <https://doi.org/10.1016/j.isprsjprs.2019.10.011>.
- Hauglin, M., Gobakken, T., Astrup, R., Ene, L., Næsset, E., 2014. Estimating single-tree crown biomass of Norway spruce by airborne laser scanning: a comparison of methods with and without the use of terrestrial laser scanning to obtain the ground reference data. *Forests* 5, 384–403. <https://doi.org/10.3390/f5030384>.
- Hauglin, M., Hansen, E.H., Næsset, E., Busterud, B.E., Gjevestad, J.G.O., Gobakken, T., 2017. Accurate single-tree positions from a harvester: a test of two global satellite-based positioning systems. *Scand. J. For. Res.* 32, 774–781. <https://doi.org/10.1080/02827581.2017.1296967>.
- Hauglin, M., Hansen, E., Sørgård, E., Næsset, E., Gobakken, T., 2018. Utilizing accurately positioned harvester data: modelling forest volume with airborne laser scanning. *Can. J. For. Res.* 48, 913–922. <https://doi.org/10.1139/cjfr-2017-0467>.
- He, K., Zhang, X., Ren, S., Sun, J., 2016. Deep residual learning for image recognition. In: Proceedings of the IEEE Computer Society Conference on Computer Vision and Pattern Recognition. <https://doi.org/10.1109/CVPR.2016.90>.
- Henning, J.G., Radtke, P.J., 2006. Detailed stem measurements of standing trees from ground-based scanning lidar. *For. Sci.* 52, 67–80.
- Hilker, T., van Leeuwen, M., Coops, N.C., Wulder, M.A., Newnham, G.J., Jupp, D.L.B., Culvenor, D.S., 2010. Comparing canopy metrics derived from terrestrial and airborne laser scanning in a Douglas-fir dominated forest stand. *Trees Struct. Funct.* 24, 819–832. <https://doi.org/10.1007/s00468-010-0452-7>.
- Holm, S., Nelson, R., Ståhl, G., 2017. Hybrid three-phase estimators for large-area forest inventory using ground plots, airborne lidar, and space lidar. *Remote Sens. Environ.* 197, 85–97. <https://doi.org/10.1016/j.rse.2017.04.004>.
- Holmgren, J., Lindberg, E., Olofsson, K., Persson, Henrik J., 2022. Tree crown segmentation in three dimensions using density models derived from airborne laser scanning. *Remote Sens. Lett.* <https://doi.org/10.1080/01431161.2021.2018149>.
- Holopainen, M., Väistö, M., Rasinmaa, J., Haapanen, R., Kalliovirta, J., Melkas, T., Yu, X., Hyppä, J., 2010. Uncertainty in timber assortment estimates predicted from forest inventory data. *Eur. J. For. Res.* 129, 1131–1142. <https://doi.org/10.1007/s10342-010-0401-4>.
- Hosoi, F., Nakai, Y., Omasa, K., 2010. Estimation and error analysis of woody canopy leaf area density profiles using 3-d airborne and ground-based scanning lidar remote-sensing techniques. *IEEE Trans. Geosci. Remote Sens.* 48, 2215–2223. <https://doi.org/10.1109/TGRS.2009.2038372>.
- Huber, P.J., 1981. *Robust Statistics*. Wiley, New York.
- Hyppä, E., Kukko, A., Kaartulou, R., White, J.C., Wulder, M.A., Pyörälä, J., Liang, X., Yu, X., Wang, Y., Kaartinen, H., 2020. Accurate derivation of stem curve and volume using backpack mobile laser scanning. *ISPRS J. Photogramm. Remote Sens.* 161, 246–262. <https://doi.org/10.1016/j.isprsjprs.2020.01.018>.
- Kaiser, L., 1983. Unbiased estimation in line-intercept sampling. *Biometrics* 39, 965–976.
- Kangas, A., Astrup, R., Breidenbach, J., Fridman, J., Gobakken, T., Korhonen, K.T., Maltamo, M., Nilsson, M., Nord-Larsen, T., Næsset, E., Olsson, H., 2018. Remote sensing and forest inventories in Nordic countries—roadmap for the future. *Scand. J. For. Res.* 33, 397–412. <https://doi.org/10.1080/02827581.2017.1416666>.
- Kankare, V., Liang, X., Väistö, M., Yu, X., Holopainen, M., Hyppä, J., 2015. Diameter distribution estimation with laser scanning based multisource single tree inventory. *ISPRS J. Photogramm. Remote Sens.* 108, 161–171. <https://doi.org/10.1016/j.isprsjprs.2015.07.007>.
- Kemmerer, J., Labelle, E.R., 2021. Using harvester data from on-board computers: a review of key findings, opportunities and challenges. *Eur. J. For. Res.* 140, 1–17. <https://doi.org/10.1007/s10342-020-01313-4>.
- Kiljunen, N., 2002. Estimating dry mass of logging residues from final cuttings using a harvester data management system. *Int. J. For. Eng.* 13, 17–25. <https://doi.org/10.1080/14942119.2002.10702452>.
- Kotivuori, E., Korhonen, L., Packalen, P., 2016. Nationwide airborne laser scanning based models for volume, biomass and dominant height in Finland. *Silva Fenn.* 50, 1–28.
- Lecun, Y., Bottou, L., Bengio, Y., Haffner, P., 1998. Gradient-based learning applied to document recognition. *Proc. IEEE* 2278–2324.
- Liang, X., Kankare, V., Yu, X., Hyppä, J., Holopainen, M., 2014. Automated stem curve measurement using terrestrial laser scanning. *IEEE Trans. Geosci. Remote Sens.* 52, 1–10.
- Liang, X., Kankare, V., Hyppä, J., Wang, Y., Kukko, A., Haggrén, H., Yu, X., Kaartinen, H., Jaakkola, A., Guan, F., Holopainen, M., Väistö, M., 2016. Terrestrial laser scanning in forest inventories. *ISPRS J. Photogramm. Remote Sens.* 115, 63–77. <https://doi.org/10.1016/j.isprsjprs.2016.01.006>.
- Lindberg, E., Holmgren, J., 2017. Individual tree crown methods for 3D data from remote sensing. *Curr. For. Rep.* 3, 19–31. <https://doi.org/10.1007/s40725-017-0051-6>.
- Lindberg, E., Holmgren, J., Olofsson, K., Olsson, H., 2012. Estimation of stem attributes using a combination of terrestrial and airborne laser scanning. *Eur. J. For. Res.* 131, 1917–1931. <https://doi.org/10.1007/s10342-012-0642-5>.
- Liu, L., Zhang, A., Xiao, S., Hu, S., He, N., Pang, H., Zhang, X., Yang, S., 2021. Single tree segmentation and diameter at breast height estimation with Mobile LiDAR. *IEEE Access*, 9, 12. <https://doi.org/10.1109/ACCESS.2021.3056877>.
- Lovell, J.L., Jupp, D.L.B., Culvenor, D.S., Coops, N.C., 2003. Using airborne and ground-based ranging lidar to measure canopy structure in Australian forests. *Can. J. Remote. Sens.* 29, 607–622. <https://doi.org/10.5589/m03-026>.
- Lu, K., Bi, H., Watt, D., Strandgard, M., Li, Y., 2018. Reconstructing the size of individual trees using log data from cut-to-length harvesters in *Pinus radiata* plantations: a case study in NSW, Australia. *J. For. Res.* 29, 13–33. <https://doi.org/10.1007/s11676-017-0517-1>.
- Maas, H.G., Bienert, A., Scheller, S., Keane, E., 2008. Automatic forest inventory parameter determination from terrestrial laser scanner data. *Int. J. Remote Sens.* 29, 1579–1593. <https://doi.org/10.1080/01431160701736406>.
- Marrs, J., Ni-Meister, W., 2019. Machine learning techniques for tree species classification using co-registered LiDAR and hyperspectral data. *Remote Sens.* 11, 1–18. <https://doi.org/10.3390/rs11070819>.
- McRoberts, R.E., 2006. A model-based approach to estimating forest area. *Remote Sens. Environ.* 103, 56–66. <https://doi.org/10.1016/j.rse.2006.03.005>.
- McRoberts, R.E., Næsset, E., Gobakken, T., 2014. Estimation for inaccessible and non-sampled forest areas using model-based inference and remotely sensed auxiliary information. *Remote Sens. Environ.* 154, 226–233. <https://doi.org/10.1016/j.rse.2014.08.028>.
- McRoberts, R.E., Chen, Q., Domke, G.M., Ståhl, G., Saarela, S., Westfall, J.A., 2016. Hybrid estimators for mean aboveground carbon per unit area. *For. Ecol. Manag.* 378, 44–56. <https://doi.org/10.1016/j.foreco.2016.07.007>.
- Mengesha, T., Hawkins, M., Nieuwenhuis, M., 2015. Validation of terrestrial laser scanning data using conventional forest inventory methods. *Eur. J. For. Res.* 134, 211–222. <https://doi.org/10.1007/s10342-014-0844-0>.
- Miettinen, M., Kulovesi, J., Kalmar, J., Visala, A., 2010. New measurement concept for Forest harvester head. *F. Serv. Robot. Springer Tracts Adv. Robot.* 62 <https://doi.org/10.1007/978-3-642-13408-1>.
- Mizoguchi, T., Ishii, A., Nakamura, H., 2019. Individual tree species classification based on terrestrial laser scanning using curvature estimation and convolutional neural network. *Int. arch. Photogramm. Remote Sens. Spat. Inf. Sci. ISPRS Arch.* 42, 1077–1082. <https://doi.org/10.5194/isprs-archives-XLII-2-W13-1077-2019>.
- Möller, J.J., Hannrup, B., Larsson, W., Barth, A., Arlinger, J., 2009. Ett system för beräkning och geografisk visualisering av avverkade kvantiteter skogsbränsle baserat på skördardata. Uppsala, Sweden.
- Möller, J.J., Arlinger, J., Barth, A., Bhuiyan, N., Hannrup, B., 2011. Ett system för beräkning och återföring av skördarbaserad information till skogliga register och planeringssystem. Uppsala, Sweden.
- Morin, M., Willets, M., 2020. Non-determinism in TensorFlow ResNets. *arXiv* 1–4.
- Næsset, E., 1997a. Estimating timber volume of forest stands using airborne laser scanner data. *Remote Sens. Environ.* 61, 246–253.
- Næsset, E., 1997b. Determination of mean tree height of forest stands using airborne laser scanner data. *ISPRS J. Photogramm. Remote Sens.* 52, 49–56. [https://doi.org/10.1016/S0924-2716\(97\)83000-6](https://doi.org/10.1016/S0924-2716(97)83000-6).
- Næsset, E., Gobakken, T., Holmgren, J., Hyppä, H., Hyppä, J., Maltamo, M., Nilsson, M., Olsson, H., Persson, Å., Söderman, U., Holmgren, J., Olsson, H., Hyppä, J., Persson, Å., Gobakken, T., Nilsson, M., 2004. Laser scanning of forest resources: the nordic experience. *Scand. J. For. Res.* 19, 482–499. <https://doi.org/10.1080/02827580410019553>.
- Nilsson, M., Nordkvist, K., Jonzén, J., Lindgren, N., Axensten, P., Wallerman, J., Egberth, M., Larsson, S., Nilsson, L., Eriksson, J., Olsson, H., 2017. A nationwide forest attribute map of Sweden derived using airborne laser scanning data and field data from the national forest inventory. *Remote Sens. Environ.* 194, 447–454. <https://doi.org/10.1016/j.rse.2016.10.022>.
- Noordermeer, L., Sørgård, E., Astrup, R., Næsset, E., Gobakken, T., 2021. Coupling a differential global navigation satellite system to a cut-to-length harvester operating system enables precise positioning of harvested trees. *Int. J. For. Eng.* 32, 119–127. <https://doi.org/10.1080/14942119.2021.1899686>.
- Olofsson, K., Holmgren, J., 2016. Single tree stem profile detection using terrestrial laser scanner data, flatness saliency features and curvature properties. *Forests* 7, <https://doi.org/10.3390/f7090207>.
- Olofsson, K., Holmgren, J., 2017. Tree stem and canopy biomass estimates from terrestrial laser scanning data. In: International Archives of the Photogrammetry, Remote Sensing and Spatial Information Sciences - ISPRS Archives, pp. 157–160. <https://doi.org/10.5194/isprs-archives-XLII-3-W3-157-2017>.
- Olofsson, K., Lindberg, E., Holmgren, J., 2008. A method for linking field-surveyed and aerial-detected single trees using cross correlation of position images and the optimization of weighted tree list graphs. *Proc. SilviLaser 2008*, 95–104.
- Olofsson, K., Holmgren, J., Olsson, H., 2014. Tree stem and height measurements using terrestrial laser scanning and the RANSAC algorithm. *Remote Sens.* 6, 4323–4344. <https://doi.org/10.3390/rs6054323>.
- Olschovsky, K., Mues, V., Köhl, M., 2016. Operational assessment of aboveground tree volume and biomass by terrestrial laser scanning. *Comput. Electron. Agric.* 127, 699–707. <https://doi.org/10.1016/j.compag.2016.07.030>.
- Persson, H.J., Fransson, J.E.S., 2017. Comparison between TanDEM-X and ALS based estimation of above ground biomass and tree height in boreal forests. *Scand. J. For. Res.* 32, 306–319. <https://doi.org/10.1080/02827581.2016.1220618>.
- Persson, H.J., Ståhl, G., 2020. Characterizing uncertainty in forest remote sensing studies at plot and stand level. *Remote Sens.* 12, 1–21. <https://doi.org/10.3390/rs12030505>.
- Persson, A., Holmgren, J., Söderman, U., 2002. Detecting and measuring individual trees using an airborne laser scanner. *Photogramm. Eng. Remote. Sens.* 68, 925–932.
- Peuhkurinen, J., Mehtätalo, L., Maltamo, M., 2011. Comparing individual tree detection and the areabased statistical approach for the retrieval of forest stand characteristics using airborne laser scanning in scots pine stands. *Can. J. For. Res.* 41, 583–598. <https://doi.org/10.1139/X10-223>.
- Puliti, S., Ene, L.T., Gobakken, T., Næsset, E., 2017a. Use of partial-coverage UAV data in sampling for large scale forest inventories. *Remote Sens. Environ.* 194, 115–126. <https://doi.org/10.1016/j.rse.2017.03.019>.

- Puliti, S., Saarela, S., Gobakken, T., Ståhl, G., Næsset, E., 2017b. Combining UAV and Sentinel-2 auxiliary data for forest growing stock volume estimation through hierarchical model-based inference. *Remote Sens. Environ.* 204, 485–497. <https://doi.org/10.1016/j.rse.2017.10.007>.
- Puliti, S., Dash, J.P., Watt, M.S., Breidenbach, J., Pearse, G.D., 2020. A comparison of UAV laser scanning, photogrammetry and airborne laser scanning for precision inventory of small-forest properties. *Forestry* 93, 150–162. <https://doi.org/10.1093/forestry/cpz057>.
- Raumonen, P., Kaasalainen, M., Markku, Å., Kaasalainen, S., Kaartinen, H., Vastaranta, M., Holopainen, M., Disney, M., Lewis, P., 2013. Fast automatic precision tree models from terrestrial laser scanner data. *Remote Sens.* 5, 491–520. <https://doi.org/10.3390/rs5020491>.
- Ren, J., Liu, P.J., Fertig, E., Snoek, J., Poplin, R., DePristo, M.A., Dillon, J.V., Lakshminarayanan, B., 2019. Likelihood ratios for out-of-distribution detection. *arXiv:1906.02845v2 [stat.ML]* 1–21. <https://arxiv.org/abs/1906.02845>.
- Seidel, D., Annighöfer, P., Thielman, A., Seifert, Q.E., Thauer, J., Glatthorn, J., Ehbrecht, M., Kneib, T., Ammer, C., 2021. Predicting tree species from 3D laser scanning point clouds using deep learning. *Front. Plant Sci.* 12, 1–12. <https://doi.org/10.3389/fpls.2021.635440>.
- Sipilehto, J., Lindeman, H., Väistaranta, M., Yu, X., Uusitalo, J., 2016. Reliability of the predicted stand structure for clear-cut stands using optional methods: airborne laser scanning-based methods, smartphone-based forest inventory application Trestima and pre-harvest measurement tool EMO. *Silva Fenn.* 50, 1–24.
- Ståhl, G., Holm, S., Gregoire, T.G., Gobakken, T., Næsset, E., Nelson, R., 2011. Model-based inference for biomass estimation in a LiDAR sample survey in Hedmark county, Norway. *Can. J. For. Res.* 41, 96–107. <https://doi.org/10.1139/X10-161>.
- Ståhl, G., Heikkilä, J., Petersson, H., Repola, J., 2014. Sample-based estimation of greenhouse gas emissions from forests—a new approach to account for both sampling and model errors. *For. Sci.* 60, 3–13.
- Ståhl, G., Saarela, S., Schnell, S., Holm, S., Breidenbach, J., Healey, S.P., Patterson, P.L., Magnussen, S., Næsset, E., McRoberts, R.E., Gregoire, T.G., 2016. Use of models in large-area forest surveys: comparing model-assisted, model-based and hybrid estimation. *For. Ecosyst.* 3, 5. <https://doi.org/10.1186/s40663-016-0064-9>.
- Stehman, S.V., Salzer, D.W., 2000. Estimating density from surveys employing unequal-area belt transects. *Wetlands* 20, 512–519. [https://doi.org/10.1672/0277-5212\(2000\)020<0512:EDFSEU>2.0.CO;2](https://doi.org/10.1672/0277-5212(2000)020<0512:EDFSEU>2.0.CO;2).
- Sumnall, M.J., Albaugh, T.J., Carter, D.R., Cook, R.L., Hession, C., Otávio, C.C., Rubilar, R.A., Wynne, R.H., Thomas, V.A., 2021. Effect of airborne laser scanning pulse density on accuracy in quantifying forest structure using an unmanned aerial vehicle. In: Silvilaser 2021. Vienna, Austria, pp. 1–3.
- Terry, L., Calders, K., Disney, M., Origo, N., Malhi, Y., Newnham, G., Raumanen, P., Åkerblom, M., Verbeeck, H., 2020. Tree species classification using structural features derived from terrestrial laser scanning. *ISPRS J. Photogramm. Remote Sens.* 168, 170–181. <https://doi.org/10.1016/j.isprsjprs.2020.08.009>.
- Thies, M., Pfeifer, N., Winterhalder, D., Gorte, B.G.H., 2004. Three-dimensional reconstruction of stems for assessment of taper, sweep and lean based on laser scanning of standing trees. *Scand. J. For. Res.* 19, 571–581. <https://doi.org/10.1080/02827580410019562>.
- Tomppo, E., Kuusinen, N., Mäkisara, K., Katila, M., Ronald, E., 2017. Effects of field plot configurations on the uncertainties of ALS-assisted forest resource estimates. *Scand. J. For. Res.* 32, 488–500. <https://doi.org/10.1080/02827581.2016.1259425>.
- Valbuena, R., Mauro, F., Rodriguez-Solano, R., Manzanera, J.A., 2010. Accuracy and precision of GPS receivers under forest canopies in a mountainous environment. *Span. J. Agric. Res.* 8, 1047–1057. <https://doi.org/10.5424/sjar/2010084-1242>.
- Wang, Y., Lehtomäki, M., Liang, X., Pyörälä, J., Kukko, A., Jaakkola, A., Liu, J., Feng, Z., Chen, R., Hyppä, J., 2019. Is field-measured tree height as reliable as believed – a comparison study of tree height estimates from field measurement, airborne laser scanning and terrestrial laser scanning in a boreal forest. *ISPRS J. Photogramm. Remote Sens.* 147, 132–145. <https://doi.org/10.1016/j.isprsjprs.2018.11.008>.
- Waser, L., Ginzler, C., Rehush, N., 2017. Wall-To-Wall tree type mapping from countrywide airborne remote sensing surveys. *Remote Sens.* 9, 766. <https://doi.org/10.3390/rs9080766>.
- Wezyk, P., Koziol, K., Glista, M., Pierzchalski, M., 2007. Terrestrial laser scanning versus traditional forest inventory first results from the polish forests. In: *ISPRS Work. Laser Scanning 2007 Silvilaser 2007*. Finl, vol. 36, pp. 424–429.
- Wiklander, M., 2020. Classification of Tree Species from 3D Point Clouds Using Convolutional Neural Networks. Umeå University.
- Yu, X., Hyppä, J., Kaartinen, H., Maltamo, M., Hyppä, H., 2008. Obtaining plotwise mean height and volume growth in boreal forests using multi-temporal laser surveys and various change detection techniques. *Int. J. Remote Sens.* 29, 1367–1386. <https://doi.org/10.1080/01431160701736356>.
- Yu, X., Hyppä, J., Karjalainen, M., Nurminen, K., Karila, K., Kukko, A., Jaakkola, A., Liang, X., Wang, Y., Hyppä, H., Katoh, M., 2015. Comparison of laser and stereo optical, SAR and InSAR point clouds from air- and space-borne sources in the retrieval of forest inventory attributes. *Remote Sens.* 7, 15933–15954. <https://doi.org/10.3390/rs71215809>.
- Zisselman, E., Tamar, A., 2020. Deep residual flow for out of distribution detection. In: *Proceedings of the IEEE Computer Society Conference on Computer Vision and Pattern Recognition*, pp. 13991–14000. <https://doi.org/10.1109/CVPR42600.2020.01401>.